Pergamon

Int. J. Solids Structures Vol. 35, No. 17, pp. 2025–2028, 1998

0020–7683/98 $19.00 + .00

PII: S0020–7683(97)00170–4

STRESS ANALYSIS OF BIMODULUS LAMINATES USING HYBRID STRESS PLATE ELEMENTS

YI-PING TSENG and YU-CHING JIANG
Department of Civil Engineering, Tamkang University, Tamsui, Taipei, Taiwan 25137, Republic of China

(*Received* 30 *May* 1996; *in revised form* 5 *June* 1997)

Abstract—Based on first-order plate theory, a hybrid stress bimodulus Mindlin plate element is developed in this paper. Both the displacement and stress distributions of bimodulus laminated plates are determined. Since the neutral surface deviates from the geometric midplane, an iterative technique is adopted. Compared to the analytical solutions, the present results are better than those of displacement-based higher-order plate models, although only first-order theory is incorporated herein. © 1998 Elsevier Science Ltd.

INTRODUCTION

There are some materials which exhibit load-dependent elastic properties, such as aramid/rubber and polyester/rubber used in automobile tires. Their stress–strain behaviors are actually nonlinear. These nonlinearities bring difficulties into the analysis. This problem is overcome by using a piecewise linearization model. For a bimodular material, the stress–strain relation is often approximated by two straight lines, as shown in Fig. 1.

Classical lamination theory yields sufficiently accurate results only for thin composite plates, wherein transverse shear effects are neglected. Mindlin-type (first-order) theories (Mindlin, 1951) were later proposed to take these effects into account by using shear deformation correction factors or functions. For thicker laminates, there are several higher-order plate theories (Kant *et al.*, 1977; Lo *et al.*, 1988) that consider these effects without the correction factors. Generally speaking, more accurate results are reported for higher-order theory than for classical and first-order theories.

There have been only a few investigations reported in the literature to study the bending analysis of bimodulus plates, and none for the stress analysis. The classical plate theory was used by Bert (1979). Mindlin plate theory was adopted by Bert *et al.* (1981) and Turvey (1984). Fung and Doong (1988) extended the study of bimodular laminates by using a higher-order plate theory. On the other hand, results from finite element analysis can be found in Reddy and Chao (1980) and Bert *et al.* (1981). Displacement models and mixed models were used, respectively, in the above studies. Finite element and finite strip solutions were also presented by Tseng and Bai (1993) and Tseng and Lee (1995). Based on the refined C^1 higher-order plate theory by Reddy (1984), Gordaninejad (1989) developed a mixed bimodulus plate element. Recently, excellent results were reported by Cho *et al.* (1990) using a higher-order individual layer plate theory.

It is well known that the hybrid stress model can supply excellent results for laminates especially for the interface stress continuity. Mau *et al.* (1972) initiated the hybrid stress plate element. High accuracy and fast convergence are further improved by Spilker *et al.* (1980) and Liou and Sun (1987). Unfortunately, large amounts of stress parameters are also required. Only a fixed set of parameters is used in Rao and Piening (1991) and Rao and Rao (1992). Their theory is attractive in formulating the hybrid stress model.

To investigate the stress analysis of bimodulus laminates, a hybrid stress Mindlin plate element has been formulated herein according to Rao's work. The neutral surface locations are determined through an iterative method. Interlaminar stress continuity and stress-free boundary conditions are enforced since a hybrid stress model is adopted. Satisfactory

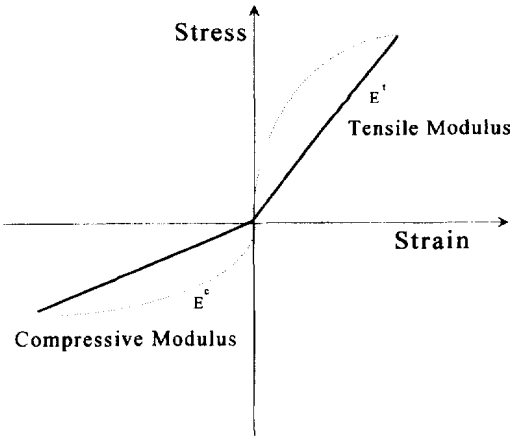

Fig. 1. Stress–strain relations of linearlized different modulus materials.

through thickness stress distributions for an ordinary (not bimodulus) material are compared to Pagano (1970). Then, the neutral surface locations and displacements of bimodulus laminated plates are found to compare with previous results. it is shown that more accurate results than for higher-order theory are obtained. Specifically, the contribution of this work is that reasonable through thickness stress distributions for bimodulus laminated plates are presented.

BIMODULUS PLATE THEORY

Consider a laminate composed of several layers of different materials in a Cartesian coordinate x, y, z with its surfaced bounded by $z = \pm h/z$; the displacement components are u, v, w in the directions of x, y, z, respectively. As shown in Fig. 2, (u_0, v_0, w_0) denote displacement components of a midplane point along the x, y, z axes, and (θ_x, θ_y) denote the rotations of a line element, originally perpendicular to the midplane plane, about the y- and x-axes. The size of laminate is a and b, the principal material axes are labeled 1, 2 and 3, and the angle θ between x and 1 axes is defined positive as shown in Fig. 2.

In Mindlin plate theory, the displacement field is represented by

$$\begin{aligned} u(x, y, z) &= u_0(x, y) - z\theta_x(x, y) \\ v(x, y, z) &= v_0(x, y) + z\theta_y(x, y) \\ w(x, y, z) &= w_0(x, y). \end{aligned} \tag{1}$$

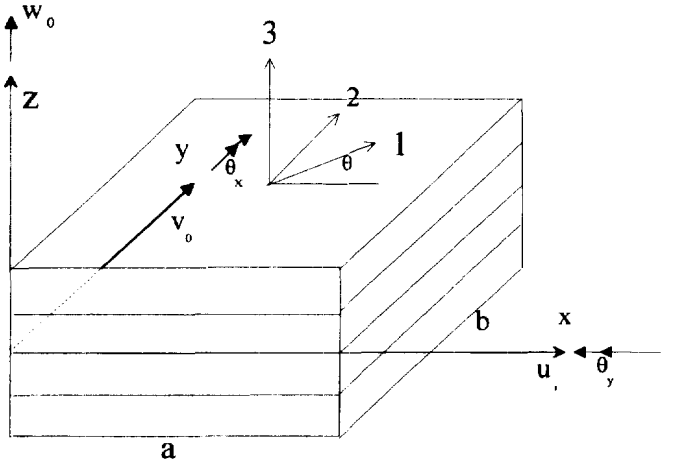

Fig. 2. Geometric shape of laminated plates.

The above equation is expressed in matrix form as

$$\{\Delta\} = [L]\{d\} \tag{2}$$

where $[L]$ is a proper differentiation operator, $\{\Delta\} = [u, v, w]^T$ is the three-dimensional displacement field, and $\{d\} = [u_0, v_0, w_0, \theta_x, \theta_y]^T$ is the midplane displacement field.

Based on small deformation theory, the strains can be constructed as

$$\begin{aligned}
\varepsilon_x &= u_{,x} = u_{0,x} + z\theta_{x,x} \\
\varepsilon_y &= v_{,y} = v_{0,y} + z\theta_{y,y} \\
\varepsilon_z &= w_{,z} = 0 \\
\gamma_{yz} &= v_{,z} w_{,y} = w_{0,y} + \theta_y \\
\gamma_{xz} &= u_{,z} + w_{,x} = w_{0,x} + \theta_x \\
\gamma_{xy} &= u_{,y} + v_{,x} = (u_{0,y} + v_{0,x}) + z(\theta_{x,y} + \theta_{y,x}).
\end{aligned} \tag{3}$$

Equations (3) are then rewritten in matrix form as

$$\{\varepsilon\} = [\bar{B}]\{d\} \tag{4}$$

where $\{\varepsilon\} = [\varepsilon_x, \varepsilon_y, \gamma_{yz}, \gamma_{xz}, \gamma_{xy}]^T$ are the strains, and $[\bar{B}]$ is a proper differentiation matrix.

Before the constitutive equations of a bimodulus plate are discussed, the neutral surface location z_{nx} and z_{ny} should be determined since the elastic properties are different in the tension or compression zone in a layer. By setting

$$\varepsilon_x = u_{0,x} + z\theta_{x,x} = 0, \quad \varepsilon_y = v_{0,y} + z\theta_{y,y} = 0 \tag{5}$$

the neutral surfaces are determined iteratively:

$$(z_{nx})_{i+1} = -(u_{0,x})_i/(\theta_{x,x})_i, \quad (z_{ny})_{i+1} = -(v_{0,y})_i/(\theta_{y,y})_i \tag{6}$$

where i is the index of iteration.

The different properties in tension and compression will cause a shift in the neutral surface away from the geometric midplane. The results that the bending-stretching couplings of an orthotropic material are exhibited. The constitutive relations of an ordinary composite material must be transferred into the bimodular form. For the nth layer of a laminate, the stress–strain relations can be expressed as

$$\{\sigma\}_n = [Q]_n\{\varepsilon\}_n \tag{7}$$

where $\{\sigma\} = [\sigma_x, \sigma_y, \tau_{yz}, \tau_{xz}, \tau_{xy}]^T$ are the stresses, and $[Q]$ is the stiffness moduli, the same as in Fung and Doong (1988).

Correspondingly, the strain–stress relations are

$$\{\varepsilon\}_n = [S]_n\{\sigma\}_n \tag{8}$$

where $[S] = [Q]^{-1}$ are the compliance moduli.

FINITE ELEMENT FORMULATION

The five displacement functions $(u_0, v_0, w_0, \theta_x, \theta_y)$ for the Mindlin plate element are interpolated by their nodal values with shape functions. Since the four-node bilinear isoparametric element is developed in this paper, the displacements are represented by

$$u_0 = \sum_{i=1}^{\text{nel}} N_i u_{0i}, \quad \theta_x = \sum_{i=1}^{\text{nel}} N_i \theta_{xi},$$

$$v_0 = \sum_{i=1}^{\text{nel}} N_i v_{0i}, \quad \theta_y = \sum_{i=1}^{\text{nel}} N_i \theta_{yi},$$

$$w_{0i} = \sum_{i=1}^{\text{nel}} N_i w_{0i}. \tag{9}$$

In matrix form, eqn (9) becomes

$$\{d\} = [N]\{q\} = \sum_{i=1}^{\text{nel}} [N_i]\{q_i\} \tag{10}$$

where nel is the number of nodes, $\{q\} = \{u_{0i}, v_{0i}, w_{0i}, \theta_{xi}, \theta_{yi}\}^{\mathrm{T}}$ are the nodal displacements for the ith node, $[N]$ is the C^0 shape function matrix, and $[N_i]$ is the ith node.

Substituting eqn (10) into the Mindlin plate displacement field (1), the three-dimensional displacements are interpolated by

$$\{\Delta\} = [L]\{d\} = [L][N]\{q\} = [\bar{N}]\{q\} = \sum_{i=1}^{\text{nel}} [\bar{N}_i]\{q_i\} \tag{11}$$

where $[\bar{N}]$, $[\bar{N}_i]$ are the shape functions matrices for the three-dimensional displacements.

The strains $\{\varepsilon\}$ are also expressed in terms of the nodal displacements $\{q\}$ by substituting eqn (10) into eqn (4):

$$\{\varepsilon\} = [\bar{B}]\{d\} = [\bar{B}][N]\{q\} = [B]\{q\} = \sum_{i=1}^{\text{nel}} [B_i]\{q_i\} \tag{12}$$

where $[B]$, $[B_i]$ are the interpolation relationships.

Assuming perfect bonds between laminae and traction-free boundary conditions, the stress field for the kth layer can be expressed by

$$\{\sigma^k\} = [P^k]\{\beta^k\} \tag{13}$$

where $\{\beta^k\}$ is the unknown stress parameter vector, and $[P^k]$ is the assumed stress matrix illustrated in the following and shown in the Appendix. Procedures for constructing the stress field will be discussed later.

Through dividing the nl-layered laminate into n finite elements and neglecting body forces, the Hellinger–Reissner functional becomes

$$\pi = \sum_{i=1}^{n} \sum_{k=1}^{nl} \left(\frac{1}{2} \int_{V_{ki}} \{\sigma^k\}^{\mathrm{T}} [S^k] \{\sigma^k\} \, \mathrm{d}V - \int_{V_{ni}} \{\sigma^k\}^{\mathrm{T}} \{\varepsilon^k\} \, \mathrm{d}V + \int_{S\sigma_{ni}} \{\Delta\}^{\mathrm{T}} \{\bar{T}\} \, \mathrm{d}s \right. \tag{14}$$

where V_{ki} is the volume of the kth element, $S_{\sigma ni}$ is the loaded surface area, and $\{\bar{T}\}$ are the prescribed external loadings.

Substitution of eqns (11)–(13) into eqn (14) yields

$$\pi = \sum_{i=1}^{n} \sum_{k=1}^{nl} \left(\frac{1}{2} \{\beta^i\}^T \int [P^k]^T [S^k] [P^k] \, dV \{\beta^i\} - \{\beta^i\}^T \int [P^k]^T [B] \, dV \{q^i\} \right) + \{q^i\}^T \int [\bar{N}]^T \{\bar{T}\} \, ds. \tag{15}$$

After the volume integrations, the functional becomes

$$\pi = \sum_{i=1}^{n} \left\{ \frac{1}{2} \{\beta^i\}^T [H^i] \{\beta^i\} - \{\beta^i\}^T [G^i] \{q^i\} + \{q^i\}^T \{Q^i\} \right. \tag{16}$$

where

$$[H^i] = \sum_{k=1}^{nl} \int_{V_{ni}} [P^k]^T [S^k] [P^k] \, dV, \quad [G^i] = \sum_{k=1}^{nl} \int_{V_{ni}} [P^k]^T [B] \, dV, \quad \{Q^i\} = \int_{S\sigma_{ni}} [\bar{N}]^T \{\bar{T}\} \, ds.$$

All integrations are carried out by Gaussian quadrature.

For ease of implementation, a layer assembly process is accomplished in eqn (16). The resulting equation becomes

$$\pi = \tfrac{1}{2} \{\beta\}^T [H] \{\beta\} - \{\beta\}^T [G] \{q\} + \{q\}^T \{Q\}. \tag{17}$$

After taking the variations of π with respect to the independent vectors $\{q\}$ and $\{\beta\}$, with $\delta\pi = 0$, and solving for $\{\beta\}$, the following equations are obtained

$$\{\beta\} = [H]^{-1} [G] \{q\} \tag{18}$$

$$[k] \{q\} - \{Q\} = 0 \tag{19}$$

where the element stiffness matrix is given by

$$[k] = [G]^T [H]^{-1} [G]. \tag{20}$$

An element assembly process is then introduced into eqn (19) in the usual way. Then, the global equations are readily available.

ASSUMED STRESS FIELD

A four-node Mindlin hybrid plate element has been developed. The displacement field of each layer is interpolated with bilinear shape functions. The consistent in-plane strain field can be chosen as follows:

$$\begin{aligned} \varepsilon_x &= \beta_1 + \beta_2 \xi + \beta_3 \eta + \zeta(\beta_4 + \beta_5 \xi + \beta_6 \eta) \\ \varepsilon_y &= \beta_7 + \beta_8 \xi + \beta_9 \eta + \zeta(\beta_{10} + \beta_{11} \xi + \beta_{12} \eta) \\ \gamma_{xy} &= \beta_{13} + \beta_{14} \xi + \beta_{15} \eta + \zeta(\beta_{16} + \beta_{17} \xi + \beta_{18} \eta) \end{aligned} \tag{21}$$

where ξ, η, ζ are the natural coordinates corresponding to x, y, z. The above equation can be expressed in matrix form as

$$\{\varepsilon\}_{IP} = [P'] \{\beta\} \tag{22}$$

where $\{\varepsilon\}_{IP} = [\varepsilon_x, \varepsilon_y, \gamma_{xy}]^T$ is the in-plane strain vector, and $[P']$ is a polynomial matrix.

Accordingly, the in-plane stress field for the kth layer can be obtained by substituting eqn (22) into eqn (7):

$$\{\sigma^k\}_{IP} = [Q]^k_{IP}\{\varepsilon\}_{IP} = [Q]^k_{IP}[P']\{\beta^k\} \tag{23}$$

where $\{\sigma^k\}_{IP} = [\sigma^k_x \sigma^k_y \tau^k_{xy}]^T$ is the in-plane stress vector, and $[Q^k]_{IP}$ are the material properties associated with the in-plane stress and strain.

Based on the in-plane stress field in eqn (23), the transverse stress field is formulated through the stress equilibrium equations. After imposing interlaminar traction and traction-free boundary conditions, the final assumed stress field can be constructed, as shown in the Appendix.

NUMERICAL EXAMPLES

To demonstrate the accuracy and efficiency of the present hybrid stress bimodulus plate element, four examples are illustrated in this section. Bimodulus cross-ply orthotropic laminates, and aramid-rubber and polyester-rubber laminates subjected to sinusoidal loading are investigated.

A sinusoidally distributed transverse load

$$q(x, y) = q_0 \sin(\pi x/a) \sin(\pi y/b) \tag{24}$$

where q_0 is applied on the top surface of the laminated plates. For comparisons, the following nondimensionalizations are also employed:

$$W = \frac{100E^c_2 w(a/2, b/2, 0)}{q_0 h^3 S^4}, \quad W^* = \frac{E^c_2 w(a/2, b/2, 0)}{q_0 b^4},$$

$$(\sigma^*_x, \sigma^*_y, \tau^*_{xy}) = \frac{1}{q_0 h^3 S^2}(\sigma_x, \sigma_y, \tau_{xy}), \quad (\tau^*_{xy}, \tau^*_{xz}) = \frac{1}{q_0 S}(\tau_{yz}, \tau_{xz}), \quad S = a/h. \tag{25}$$

where a, b are the length and width, h is the thickness, and w is the maximum displacement at the center of the plate. As for the through thickness distributions σ_x, σ_y are located at the plate center $(a/2, b/2)$, τ_{xy} is at $(0, 0)$, τ_{yz} is at $(a/2, 0)$, and τ_{xz} is at $(0, b/2)$.

The normalized neutral surface locations are defined as

$$Z_n = z_n/h, \quad Z_{nx} = z_{nx}/h, \quad Z_{ny} = z_{ny}/h \tag{26}$$

where Z_n is the single-layer plate of isotropic material, and Z_{nx}, Z_{ny} are for two-layered cross-ply laminates of orthotropic material.

Simply-supported rectangular plates are studied. Owing to symmetry, only a quarter plate is analysed and modeled by a mesh of 6×6 elements except in the convergence study. In all examples, the maximum deflections and neutral surface locations are compared to available analytical or finite element solutions. Higher-order plate theory is adopted in an analytical solution by Fung and Doong (1988), Tseng and Bai (1993) developed a displacement-based higher-order plate element, and Cho *et al.* (1990) proposed higher-order individual-layer theory. Cho's results are thought to be the most accurate. For $E^t/E^c = 1$ ordinary material, Cho *et al.* obtained the same results as Pagano's elasticity solution (1970). It is noted that the stress analysis for bimodulus laminates are also presented, which has never been discussed in previous studies.

Example 1 : *cross-ply bimodulus laminates of orthotropic material*

The orthotropic material properties with respect to the principal material axes of each lamina are

Young's modulus (E)		Shear modulus (G)		Poisson's ratio (v)
Tension	Compression	Tension	Compression	Tension and compression
$E_1^t = 25E_2^t$	$E_1^c = 25E_2^c$	$G_{12}^t = 0.5E_2^t$	$G_{12}^c = 0.5E_2^c$	$v_{ij} = 0.25$
$E_2^t = E_2^c$	$E_2^c = 1.0$	$G_{23}^t = 0.2E_2^t$	$G_{23}^c = 0.2E_2^c$	$v_{ij} = v_{ji}E_i/E_j$
$E_3^t = E_2^t$	$E_3^c = E_2^c$	$G_{13}^t = 0.5E_2^t$	$G_{13}^c = 0.5E_2^c$	$(i \neq j, i,j = 1,2,3)$

Table 1 lists the present results for (0°/90°) bimodulus $a/h = 10$ thick laminates with other available solutions appended for ease of comparison. Very close results are observed for Tseng and Bai (1993) and Fung and Doong (1988), since both used higher-order theory. The present study reveals similar tendency. It is worthwhile pointing out that the present element can provide a more accurate displacement analysis than the higher-order theory, although only the first-order theory was incorporated herein. This is due to the elegancy of the hybrid stress method in predicting accurate stress distributions. Results for $a/h = 100$ square thin plates and $a/h = 10$ thick plates are displayed in Tables 2 and 3, respectively. Similar behaviors are observed and the results of this element are in good agreement with the other solutions.

Convergence studies for the cases of $E_t/E_t = 2$ and 0.2 are shown in Fig. 3, where fast convergence is observed. Therefore, the mesh of 6×6 elements are used in all examples. Acceptable stress analyses for (0°/90°) cross-ply laminates of ordinary material are illustrated in Figs 4 and 5. Compared to Pagano's elasticity solution, the present results for an $E^t/E^c = 1$ plate satisfy interlaminar transverse stress continuity and the traction-free conditions. Figures 6 and 7 depict the through thickness stress distributions of σ_x, τ_{xz} for an $E_2^t/E_2^c = 2$ plate, and Figs 8 and 9 are σ_y, τ_{yz} for an $E_2^t/E_2^c = 0.2$ plate. The series solutions based on higher-order theory are also displayed, where the discontinuous interface transverse stresses are noted.

Table 1. Normalized maximum center deflections and neutral surface locations of orthotropic bimodular (0°/90°) square laminate under sinusoidal loading ($S = 10$, $a/b = 1.0$)

	Present (6*6)			Tseng and Bai (1993)			Fung and Doong (1988)			Cho *et al.* (1990)		
E_2^t/E_2^c	Znx	Zny	W	Znx	Zny	W	Znx	Zny	W	Znx	Zny	W
0.2	0.1374	−0.3310	3.2391	0.1389	−0.3377	3.0181	0.1364	−0.3378	3.0298	0.1280	−0.3488	3.3340
0.6	0.2030	−0.2677	1.6225	0.2053	−0.2682	1.5918	0.2036	−0.2707	1.5996	0.1979	−0.2748	1.6200
1.0	0.2353	−0.2353	1.2336	0.2387	−0.2340	1.2214	0.2372	−0.2372	1.2266	0.2351	−0.2371	1.2270
1.4	0.2566	−0.2136	1.0494	0.2608	−0.2116	1.0380	0.2593	−0.2150	1.0413	0.2601	−0.2124	1.0460
2.0	0.2789	−0.1908	0.8992	0.2838	−0.1884	0.8823	0.2824	−0.1918	0.8832	0.2862	−0.1871	0.9000

Table 2. Normalized maximum center deflections and neutral surface locations of orthotropic bimodular (0°/90°) square laminate under sinusoidal loading ($S = 100$, $a/b = 1.0$)

	Present (6*6)			Tseng and Bai			Fung and Doong			Cho *et al.*		
E_2^t/E_2^c	Znx	Zny	W	Znx	Zny	W	Znx	Zny	W	Znx	Zny	W
0.2	0.1371	−0.3295	2.5808	0.1375	−0.3333	2.6255	0.1373	−0.3332	2.6249	—	—	—
2.0	0.2790	−0.1907	0.7664	0.2792	−0.1912	0.7674	0.2971	−0.1914	0.7667	0.2792	−0.1914	0.7677

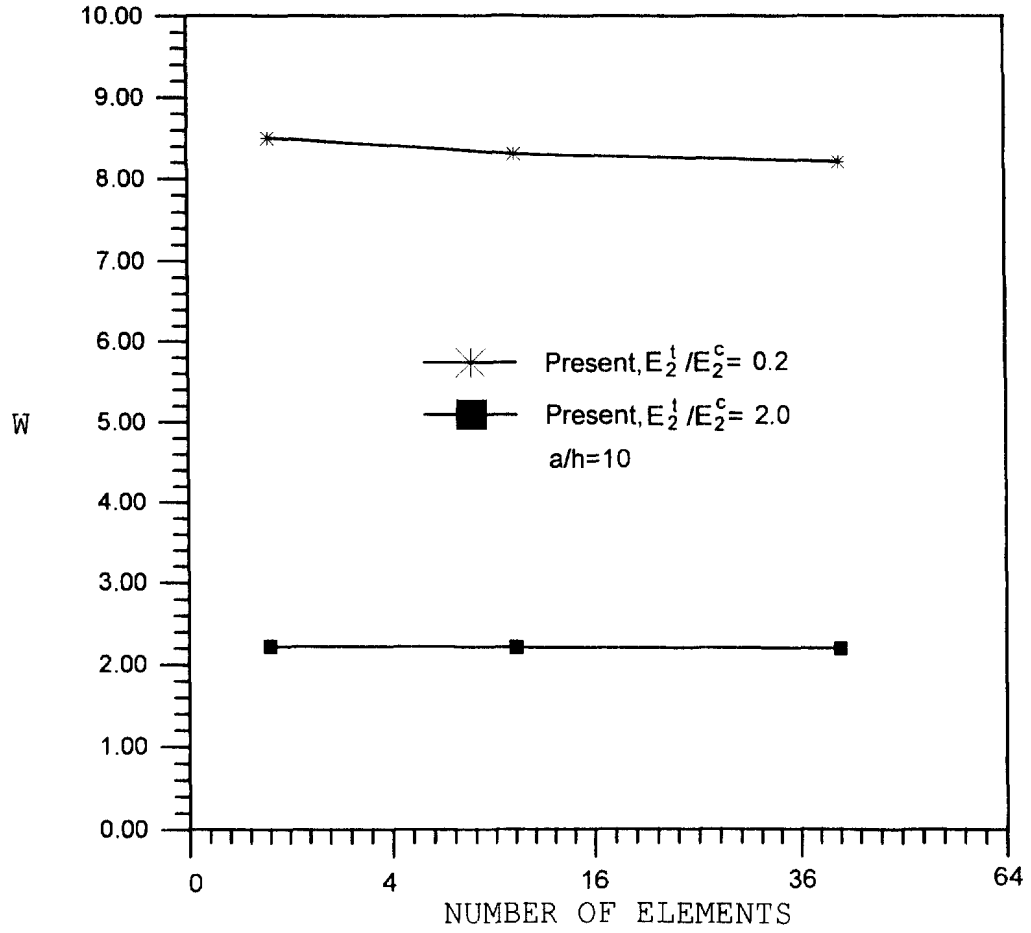

Fig. 3. Convergence studies for isotropic single plates.

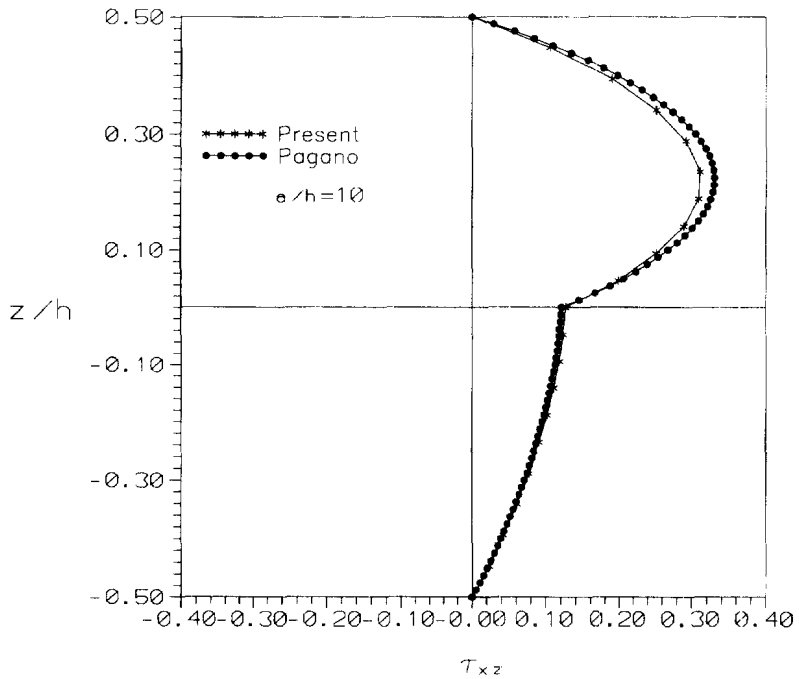

Fig. 4. $\tau_{xz}^*(0, b/2, z)$ for two-layer cross-ply ordinary laminate.

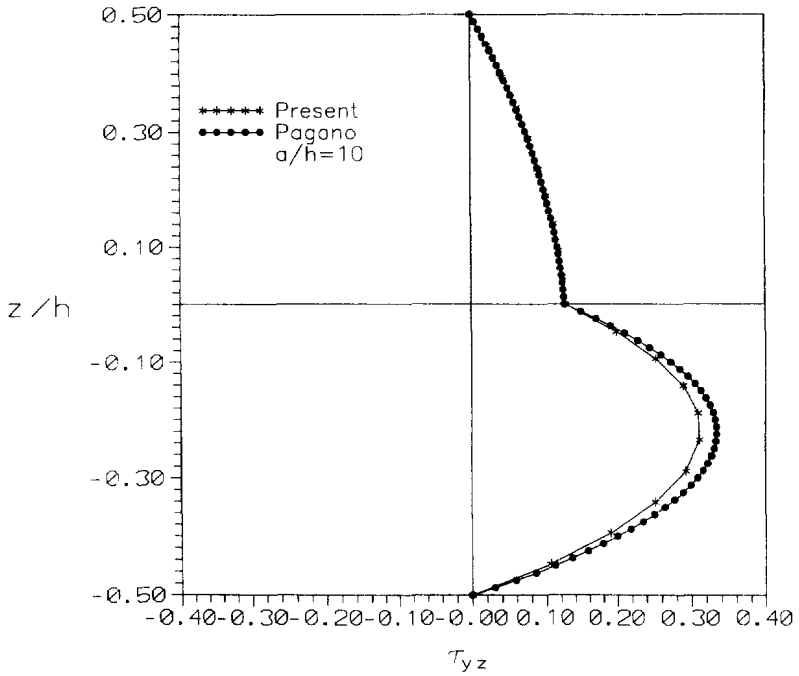

Fig. 5. $\tau_{yz}^{*}(a/2, 0, z)$ for two-layer cross-ply ordinary laminate.

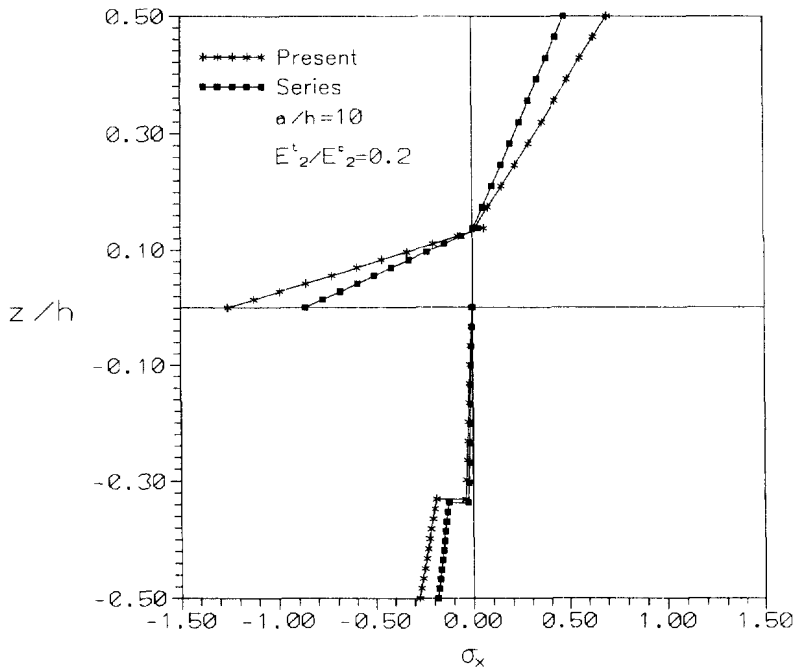

Fig. 6. $\sigma_{x}^{*}(0, b/2, z)$ for two-layer cross-ply bimodular laminate.

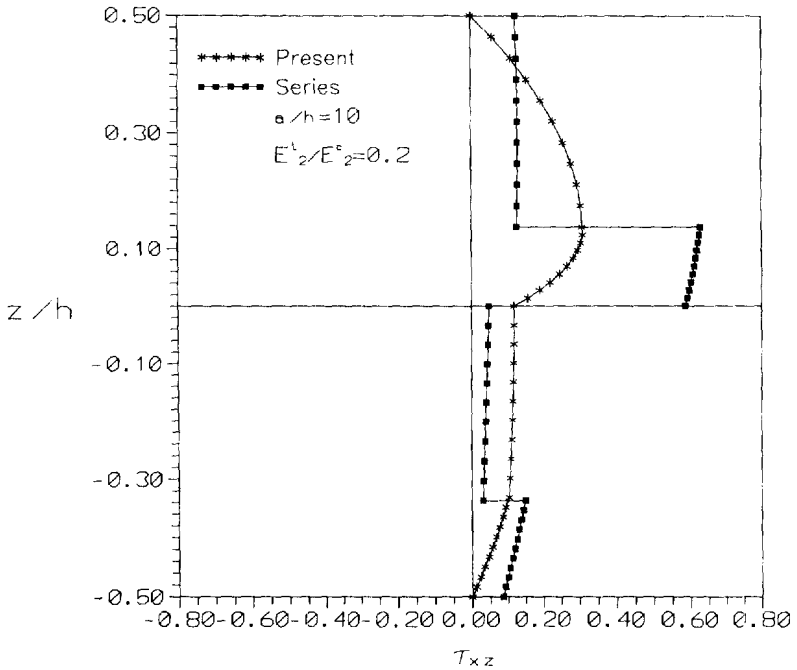

Fig. 7. $\tau_{xz}^{*}(0, b/2, z)$ for two-layer cross-ply bimodular laminate.

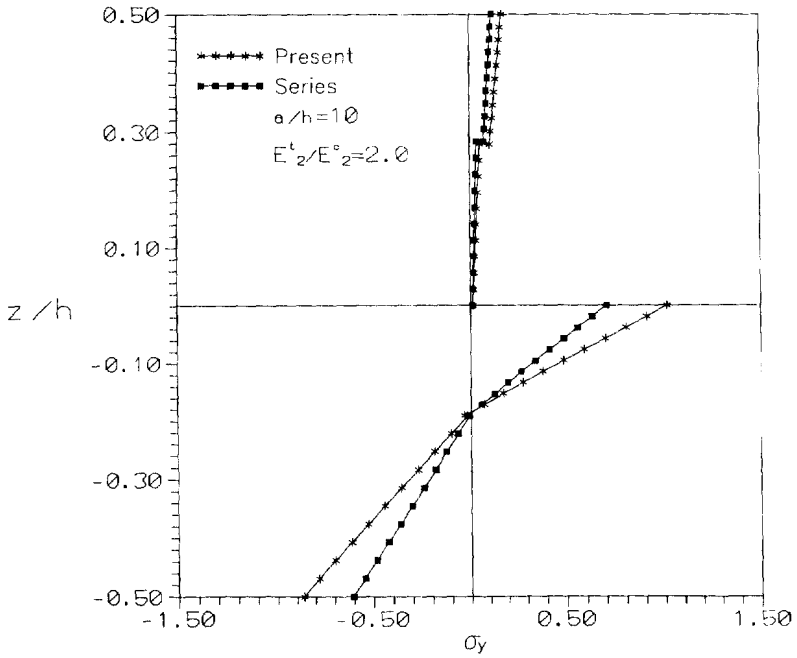

Fig. 8. $\sigma_{y}^{*}(0, b/2, z)$ for two-layer cross-ply bimodular laminate.

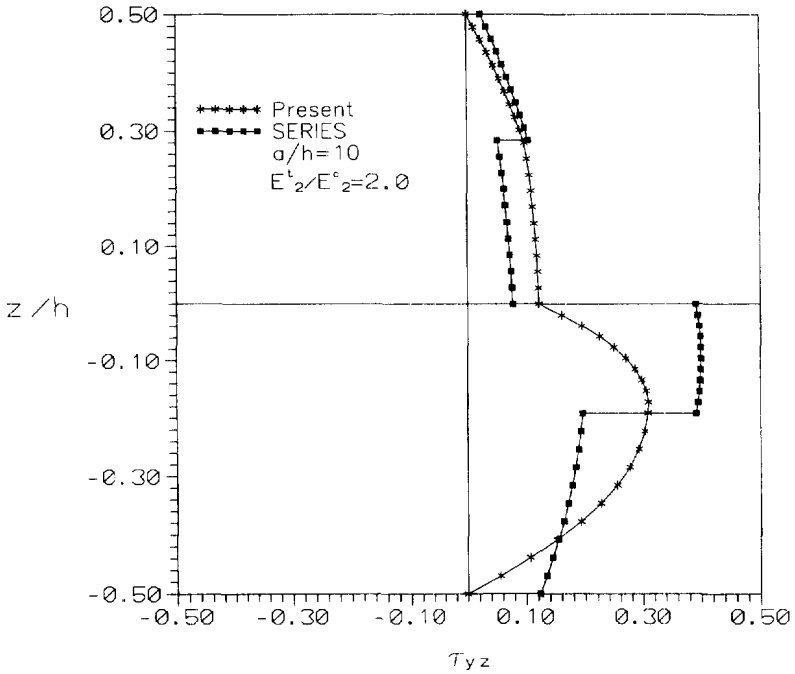

Fig. 9. $\tau_{yz}^{*}(0, b/2, z)$ for two-layer cross-ply bimodular laminate.

Table 3. Normalized maximum center deflections and neutral surface locations of orthotropic bimodular (0°/90°) rectangular laminate under sinusoidal loading ($S = 10$, $a/b = 0.3$)

	Present (6*6)			Tseng and Bai			Fung and Doong			Cho *et al.*		
E_2^t/E_2^c	*Znx*	*Zny*	*W*	*Znx*	*Zny*	*W*	*Znx*	*Zny*	*W*	*Znx*	*Zny*	*W*
0.2	0.1341	−0.3315	7.3474	0.1347	−0.3600	7.0450	0.1344	−0.3600	70.606	—	—	—
2.0	0.2746	−0.2038	2.0636	0.2774	−0.2079	2.0214	0.2765	−0.2153	2.0172	0.2083	−0.2201	2.0420

Example 2 : *aramid-rubber and polyester-rubber*

Two actual bimodular materials used in automobile tires are aramid-rubber and polyester-rubber, whose material properties are

Aramid-rubber	Tension	Compression
Young's modulus (E)	$E_1^t = 3.58$	$E_1^c = 0.0120$
	$E_2^t = E_3^t = 0.00909$	$E_2^c = E_3^c = 0.0120$
Shear modulus (G)	$G_{12}^t = G_{13}^t = 0.00370$	$G_{12}^c = G_{13}^c = 0.00370$
	$G_{23}^t = 0.00290$	$G_{23}^c = 0.00499$
Poisson's ratio (v)	$v_{12}^t = v_{13}^t = 0.415$	$v_{12}^c = v_{13}^c = 0.205$
Polyester-rubber	Tension	Compression
Young's modulus (E)	$E_1^t = 0.617$	$E_1^c = 0.0369$
	$E_2^t = E_3^t = 0.0080$	$E_2^c = E_3^c = 0.0106$
Shear modulus (G)	$G_{12}^t = G_{13}^t = 0.00262$	$G_{12}^c = G_{13}^c = 0.00262$
	$G_{23}^t = 0.00233$	$G_{23}^c = 0.00475$
Poisson's ratio (v)	$v_{12}^t = v_{13}^t = 0.475$	$v_{12}^c = v_{13}^c = 0.185$

Table 4. Normalized maximum center deflections and neutral surface locations of aramid-rubber (0°/90°) laminate under sinusoidal loading ($S = 100$)

	Present (6*6)			Tseng and Bai			C.F.			F.E.		
a/h	Znx	Zny	W^*	Znx	Zny	W^*	Znx	Zny	W^*	Znx	Zny	W^*
0.5	0.4435	−0.0721	0.00182	0.4434	−0.0724	0.00181	0.4438	−0.0714	0.00181	0.4390	−0.0720	0.00180
0.7	0.4418	−0.0515	0.00594	0.4417	−0.0516	0.00592	0.4423	−0.0517	0.00593	0.4419	−0.0530	0.00588
1.0	0.4384	−0.0357	0.01778	0.4383	−0.0358	0.01771	0.4389	−0.0355	0.01780	0.4392	−0.0371	0.01761
1.4	0.4325	−0.0253	0.03956	0.4326	−0.0252	0.03939	0.4332	−0.0249	0.03961	0.4334	−0.0259	0.03917
2.0	0.4218	−0.0177	0.06903	0.4220	−0.0176	0.06869	0.4228	−0.0182	0.06894	0.4229	−0.0182	0.06826

C.F.: closed-form solution (Reddy and Chao, 1980).
F.E.: finite element solution (Reddy and Chao, 1980).

Table 5. Normalized maximum center deflections and neutral surface locations of polyester-rubber (0°/90°) laminate under sinusoidal loading ($S = 100$)

	Present (6*6)			Tseng and Bai			C.F.			F.E.		
a/h	Znx	Zny	W^*	Znx	Zny	W^*	Znx	Zny	W^*	Znx	Zny	W^*
0.5	0.3600	−0.1401	0.00192	0.3649	−0.1411	0.00190	0.3650	−0.1412	0.00190	0.3719	−0.1310	0.00189
0.7	0.3634	−0.1135	0.00625	0.3635	−0.1138	0.00622	0.3638	−0.1139	0.00623	0.3642	−0.1171	0.00618
1.0	0.3607	−0.0963	0.01785	0.3611	−0.0962	0.01766	0.3622	−0.0961	0.01783	0.3618	−0.0993	0.01762
1.4	0.3562	−0.0871	0.03505	0.3569	−0.0868	0.03479	0.3573	−0.0867	0.03497	0.3583	−0.0896	0.03451
2.0	0.3477	−0.0820	0.05116	0.3492	−0.0815	0.05067	0.3498	−0.0815	0.05090	0.3541	−0.0776	0.05021

Tables 4 and 5 are for $a/h = 100$ thin rectangular cross-ply laminates. The predicted results are quite accurate, compared to the results by Reddy and Chao (1980) and Tseng and Bai (1993). The deviation is under 2%.

CONCLUSIONS

Several comparative benchmark problems have been presented to demonstrate the applicability and accuracy of the present Mindlin hybrid stress element in the analysis of bimodulus laminated plates. Excellent accuracy and fast convergence are observed. Moreover, the present results based on first-order theory are even better than those of higher-order theory. This implies that the transverse shear stress are significant factor for composite laminates. The presented through thickness stress distributions for bimodulus laminates are believed to be reasonable.

REFERENCES

Bert, C. W. (1977) Models for fibrous composites with different properties in tension and compression. *Journal of Engineering Material Technology* **99**(4), 344–349.

Bert, C. W. (1979) Classical analysis of laminated bimodulus composite-material plates. University of Oklahoma, School of Aerospace, Mechanical and Nuclear Engineering, Contract no. 0014-7b-C-0647, Report OU-AMNE-79-10A.

Bert, C. W., Reddy, J. N. and Reddy, V. S. and Chao, W. C. (1981) Bending of thick rectangular plates laminated of bimodulus composite materials. *AIAA Journal* **19**(10), 1342–1349.

Cho, K. N., Striz, A. G. and Bert, C. W. (1990) Bending analysis of thick bimodular laminates by higher-order individual-layer theory. *Composite Structures* **15**, 1–24.

Fung, C. P. and Doong, J. L. (1988) Bending of a bimodulus laminated plate based on a higher-order shear deformation theory. *Composite Structures* **10**(2), 121–144.

Gordaninejad, F. (1989) Effect of shear deformation on bending of bimodular composite-material plates. *Composite Structures* **12**, 161–170.

Kant, T. and Pandya, B. N. (1988) A simple finite element formulation of a higher-order theory for unsymmetrically laminated composite plates. *Composite Structures* **9**, 215–246.

Liou, W. J. and Sun, C. T. (1987) A three-dimensional hybrid stress isoparametric element for the analysis of laminated composite plates. *Composite Structures* **25**(2), 241–251.

Lo, K. H. R., Christensen, M. and Wu, E. M. (1977) A higher-order theory of plate deformation: part 2—laminated plates. *Journal of Applied Mechanics* **44**, 669–676.

Mau, S. T., Pian, T. H. H. and Tong, P. (1972) Finite element solutions for laminated thick-plates. *Journal of Composite Materials* **6**, 304–311.

Mindlin, R. D. (1951) Influence of rotary inertia and shear on flexural motion of isotropic elastic plates. *Journal of Applied Mechanics* **18**, 31–38.

Pagano, J. N. (1970) Exact solutions for rectangular bidirectional composites and sandwich plates. *Journal of Composite Materials* **4**, 20–34.
Rao, M. and Piening, H. R. M. (1991) Analysis of sandwich plates using hybrid-stress finite element. *AIAA Journal* **29**(9), 1498–1503.
Rao, K. M. and Rao, Y. U. (1992) Computer program for the stiffness matrix of laminated plates using the hybrid-stress finite element. *Composite Structures* **45**(2), 351–363.
Reddy, J. N. and Chao, W. C. (1980) Finite element analysis of laminated bimodulus plates. *Composite Structures* **12**(2), 245–251.
Reddy, J. N. (1984) A refined nonlinear theory of plates and plates with transverse shear deformation. *Journal of Solids and Structures* **20**, 665–684.
Spilker, R. L. and Munir, N. I. (1980) A hybrid-stress quadratic serendipity displacement Mindlin plate bending element. *Composite Structures* **12**, 11–21.
Tseng, Y. P. and Bai, K. P. (1993) Bending analysis of bimodular laminates using a higher-order plate theory with the finite element technique. *Composite Structures* **47**(3), 487–494.
Tseng, Y. P. and Lee, C T. (1995) Bending analysis of bimodular laminates using a higher-order finite strip method. *Composite Structures* **30**, 341–350.
Turvey, G. J. (1984) On the flexural response of moderately thick bimodular laminated plates on elastic foundations. *Composite structures* **2**, 23–47.

APPENDIX

The formulated stress field for a two-layer bimodulus laminated plate is

$$
[P^k] = \begin{bmatrix}
Q^k_{11} & Q^k_{11}\xi & Q^k_{11}\eta & Q^k_{11}\zeta & Q^k_{11}\xi\zeta & Q^k_{11}\eta\zeta \\
Q^k_{12} & Q^k_{12}\xi & Q^k_{12}\eta & Q^k_{12}\zeta & Q^k_{12}\xi\zeta & Q^k_{12}\eta\zeta \\
0 & C^k_{yz2}-Q^k_{16}\zeta & C^k_{yz3}-Q^k_{12}\zeta & 0 & C^k_{yz5}-Q^k_{16}\dfrac{\zeta^2}{2} & C^k_{yz6}-Q^k_{12}\dfrac{\zeta^2}{2} \\
0 & C^k_{xz2}-Q^k_{11}\zeta & C^k_{xz3}-Q^k_{16}\zeta & 0 & C^k_{xz5}-Q_{11}\dfrac{\zeta^2}{2} & C^k_{xz6}-Q^k_{16}\dfrac{\zeta^2}{2} \\
Q^k_{16} & Q^k_{16}\xi & Q^k_{16}\eta & Q^k_{16}\zeta & Q^k_{16}\xi\zeta & Q^k_{16}\eta\zeta \\
Q^k_{12} & Q^k_{12}\xi & Q^k_{12}\eta & Q^k_{12}\zeta & Q^k_{12}\xi\zeta & Q^k_{12}\eta\zeta \\
Q^k_{22} & Q^k_{22}\xi & Q^k_{22}\eta & Q^k_{22}\zeta & Q^k_{22}\xi\zeta & Q^k_{22}\eta\zeta \\
0 & C^k_{yz8}-Q^k_{26}\zeta & C^k_{yz9}-Q^k_{22}\zeta & 0 & C^k_{yz11}-Q^k_{26}\dfrac{\zeta^2}{2} & C^k_{yz12}-Q^k_{22}\dfrac{\zeta^2}{2} \\
0 & C^k_{xz8}-Q^k_{12}\zeta & C^k_{xz9}-Q^k_{26}\zeta & 0 & C^k_{xz11}-Q^k_{12}\dfrac{\zeta^2}{2} & C^k_{xz12}-Q^k_{26}\dfrac{\zeta^2}{2} \\
Q^k_{26} & Q^k_{26}\xi & Q^k_{26}\eta & Q^k_{26}\zeta & Q^k_{26}\xi\zeta & Q^k_{26}\eta\zeta \\
Q^k_{16} & Q^k_{16}\xi & Q^k_{16}\eta & Q^k_{16}\zeta & Q^k_{16}\xi\zeta & Q^k_{16}\eta\zeta \\
Q^k_{26} & Q^k_{26}\xi & Q^k_{26}\eta & Q^k_{26}\zeta & Q^k_{26}\xi\zeta & Q^k_{26}\eta\zeta \\
0 & C^k_{yz14}-Q_{66}\zeta & C^k_{yz15}-Q^k_{26}\zeta & 0 & C^k_{yz17}-Q^k_{66}\dfrac{\zeta^2}{2} & C^k_{yz18}-Q^k_{26}\dfrac{\zeta^2}{2} \\
0 & C^k_{xz14}-Q^k_{16}\zeta & C^k_{xz15}-Q^k_{66}\zeta & 0 & C^k_{xz17}-Q^k_{16}\dfrac{\zeta^2}{2} & C^k_{xz18}-Q^k_{66}\dfrac{\zeta^2}{2} \\
Q^k_{66} & Q^k_{66}\xi & Q^k_{66}\eta & Q^k_{66}\zeta & Q^k_{66}\xi\zeta & Q^k_{66}\eta\zeta
\end{bmatrix}
$$

where C^k_{xzi} and C^k_{yzi} are constants.

For the first layer, the constants are

$$
\begin{Bmatrix} C^1_{xz} \\ C^1_{yz} \end{Bmatrix} = \begin{bmatrix}
0 & h_1Q^1_{11} & h_1Q^1_{16} & 0 & \dfrac{h_1^2}{2}Q^1_{11} & \dfrac{h_1^2}{2}Q^1_{16} \\
0 & h_1Q^1_{16} & h_1Q^1_{12} & 0 & \dfrac{h_1^2}{2}Q^1_{16} & \dfrac{h_1^2}{2}Q^1_{12} \\
0 & h_1Q^1_{12} & h_1Q^1_{26} & 0 & \dfrac{h_1^2}{2}Q^1_{12} & \dfrac{h_1^2}{2}Q^1_{26} \\
0 & h_1Q^1_{26} & h_1Q^1_{22} & 0 & \dfrac{h_1^2}{2}Q^1_{26} & \dfrac{h_1^2}{2}Q^1_{22}
\end{bmatrix}
\begin{bmatrix}
0 & h_1Q^1_{16} & h_1Q^1_{66} & 0 & \dfrac{h_1^2}{2}Q^1_{16} & \dfrac{h_1^2}{2}Q^1_{66} \\
0 & h_1Q^1_{66} & h_1Q^1_{26} & 0 & \dfrac{h_1^2}{2}Q^1_{66} & \dfrac{h_1^2}{2}Q^1_{26}
\end{bmatrix}
$$

For the 2nd–kth layer, the recurrence formulas for the constants are

$$\begin{Bmatrix} C_{xz}^{k} \\ C_{yz}^{k} \end{Bmatrix} = \begin{Bmatrix} C_{xz}^{k-1} \\ C_{yz}^{k-1} \end{Bmatrix} +$$

$$\begin{bmatrix} 0 & h_i(Q_{11}^{k}-Q_{11}^{k-1}) & h_i(Q_{16}^{k}-Q_{16}^{k-1}) & 0 & \frac{h_i^2}{2}(Q_{11}^{k}-Q_{11}^{k-1}) & \frac{h_i^2}{2}(Q_{16}^{k}-Q_{16}^{k-1}) \\ 0 & h_i(Q_{16}^{k}-Q_{16}^{k-1}) & h_i(Q_{12}^{k}-Q_{12}^{k-1}) & 0 & \frac{h_i^2}{2}(Q_{16}^{k}-Q_{16}^{k-1}) & \frac{h_i^2}{2}(Q_{12}^{k}-Q_{12}^{k-1}) \\ 0 & h_i(Q_{12}^{k}-Q_{12}^{k-1}) & h_i(Q_{26}^{k}-Q_{26}^{k-1}) & 0 & \frac{h_i^2}{2}(Q_{12}^{k}-Q_{12}^{k-1}) & \frac{h_i^2}{2}(Q_{26}^{k}-Q_{26}^{k-1}) \\ 0 & h_i(Q_{26}^{k}-Q_{26}^{k-1}) & h_i(Q_{22}^{k}-Q_{22}^{k-1}) & 0 & \frac{h_i^2}{2}(Q_{26}^{k}-Q_{26}^{k-1}) & \frac{h_i^2}{2}(Q_{22}^{k}-Q_{22}^{k-1}) \\ 0 & h_i(Q_{16}^{k}-Q_{12}^{k-1}) & h_i(Q_{66}^{k}-Q_{66}^{k-1}) & 0 & \frac{h_i^2}{2}(Q_{16}^{k}-Q_{16}^{k-1}) & \frac{h_i^2}{2}(Q_{66}^{k}-Q_{66}^{k-1}) \\ 0 & h_i(Q_{66}^{k}-Q_{66}^{k-1}) & h_i(Q_{26}^{k}-Q_{26}^{k-1}) & 0 & \frac{h_i^2}{2}(Q_{66}^{k}-Q_{66}^{k-1}) & \frac{h_i^2}{2}(Q_{26}^{k}-Q_{26}^{k-1}) \end{bmatrix}$$

where h_i is the thickness of the ith lamina.